Transp Porous Med (2011) 87:603–623
DOI 10.1007/s11242-010-9704-7

Probability Density Function Modeling of Multi-Phase Flow in Porous Media with Density-Driven Gravity Currents

Manav Tyagi · Patrick Jenny

Received: 25 March 2010 / Accepted: 21 December 2010 / Published online: 5 February 2011

Abstract A probability density function (PDF) based approach is employed to model multi-phase flow with interfacial mass transfer (dissolution) in porous media. The joint flow statistics is represented by a mass density function (MDF), which is transported in the physical and probability spaces via Fokker–Planck equation. This MDF-equation requires Lagrangian evolutions of the random flow variables; these evolutions are stochastic processes honoring the micro-scale flow physics. To demonstrate the concept, we consider an example of immiscible two-phase flow with the non-equilibrium dissolution of single component from one phase into the other-a model for solubility trapping during CO_2 storage in brine aquifer. Since CO_2-rich brine is denser than pure brine, density-driven countercurrent flow is set up in the brine phase. The stochastic models mimicking the physics of countercurrent flow lead to a modeled MDF-equation, which is solved using our recently developed stochastic particle method for multi-phase flow (Tyagi et al. J Comput Phys 227:6696–6714, 2008). In addition, we derive Eulerian equations for stochastic moments (mean, variance, etc.) and show that unlike the MDF-equation the system of moment equations is not closed. In classical Darcy formulation, for example, the mean concentration equation is closed by neglecting variance. However, with several one- and two-dimensional simulations, it is demonstrated that the PDF and Darcy modeling approaches give significantly different results. While the PDF-approach properly accounts for the long correlation length scales and the concentration variance in density-driven countercurrent flow, the same phenomenon cannot be captured accurately with a standard Darcy model.

Keywords PDF-modeling · Stochastic particle method · Multi-phase flow · Dissolution · CO_2 storage

M. Tyagi (✉) · P. Jenny
Institute of Fluid Dynamics, ETH Zurich, Sonneggstrasse 3, Zurich 8092, Switzerland
e-mail: tyagi@ifd.mavt.ethz.ch

1 Introduction

A continuum description of multi-phase flow in porous media can be provided by Navier–Stokes equations that are complemented by interfacial and boundary conditions. Typical flow velocities in subsurface formations are of the order of few centimeters per day and the pore space size less than a millimeter. Under these conditions, the flow Reynolds number (Re) is much less than one; consequently, the nonlinear Navier–Stokes equations further reduce to the linear Stokes equations (Whitaker 1986a). However, based on this mathematically rigorous description, a full pore-scale simulation of multi-phase multi-component flow in a real porous medium geometry is computationally difficult to tackle; therefore, the real porous medium is often substituted by a network of pores and throats (Blunt et al. 1992). Pore-network simulations can be performed with simplified pore and throat filling rules that are derived by solving Stokes equations in the individual phases and using capillary pressure jump condition across the interface (Lenormand et al. 1988). Significant amount of work has been reported on pore-network simulations over the last three decades. This ranges from the use of simple invasion percolation theory based simulators first developed in early 1980s (Chandler et al. 1982) to the use of complex pore-networks constructed from porous matrix morphology (Blunt et al. 2002; Okabe and Blunt 2004). However, in spite of great progress in computational resources, to date pore-network simulations are feasible only for sample sizes of few centimeters. This limits the application of pore-network simulators to predict flows in subsurface formations, which typically vary from hundreds of meters to few kilometers (Bear 1979).

To be able to simulate subsurface flows in reasonable time, one, therefore, employs large-scale (up-scaled) flow models. These models predict average flow quantities, which are defined over a representative elementary volume (REV) containing large number of pores (Bear 1972). Currently, most of them employ Darcy's law that was initially proposed for single phase flow, and that later was extended to multi-phase flow, however, in a very ad hoc way (Muskat 1949). Darcy's law is essentially an equation for momentum balance relating the volume flux to the viscous pressure gradient and the gravitational head. For multi-phase flow it is often written as

$$F_a = -\frac{k_{r_a} k}{\mu_a}(\nabla p_a + \rho_a g e_z) \tag{1}$$

for the phase a, where F_a is the phase volume flux, p_a the phase pressure, g the acceleration due to gravity, ρ_a the phase density, k the rock permeability, k_{r_a} the relative permeability and μ_a the phase viscosity. The phase pressures are usually related by the capillary pressure relations, for example, in case of two-phase flow, one uses the relationship $p_1 - p_2 = P_{\mathrm{c}}$, where P_{c} is known as the macroscopic capillary pressure. Classically, both relative permeability and macroscopic capillary pressure are assumed to be functions of phase saturation and usually obtained from small scale experiments or pore-network simulation studies (Aziz and Settari 2002).

At its core, Darcy-approach assumes that one can provide a full macroscopic description of flow by knowing only the average flow quantities; the microscopic effects are lumped into empirical coefficients (e.g. the shapes of relative permeability curves depend on pore-scale dynamics (Blunt and King 1990, 1991)). However, for flows with microscopic nonlinearities this is true only if correlations are much shorter than the scales of interest. Otherwise, in general, all statistical moments are needed to provide a complete flow description. The derivations of mean equations from a micro-scale description have clearly pointed out this issue (Whitaker 1986a,b), where one encounters several unclosed terms consisting of higher

moments. Note that equations governing these higher moments would have unclosed terms containing even higher moments and so on. Thus, such a statistical description of macroscopic multiphase flow in porous media suffers from the closure problem, i.e. there exist more unknowns than equations.

The closure problem can be avoided by adopting a probability density function (PDF)—approach in which a joint PDF or a mass density function (MDF) of the flow variables is modeled. This MDF is transported in a high dimensional space (physical plus compositional) via Fokker–Planck equation (Gardiner 2004). This MDF-equation is modeled by the Lagrangian evolutions of random variables; these evolutions can be derived from the fine scale flow physics. As such PDF-approach considers an ensemble of several independent realizations at a fixed point in space at a given time. However, if one could invoke ergodicity such that this ensemble at a point in space can be approximated by an ensemble of spatially distributed realizations over an REV in the neighborhood of the point, the PDF-approach can also provide a up-scaled large-scale flow model. Note that in this case the information about the size of REV would be hidden in the stochastic model.[1]

Although an MDF-equation, in principle, can be solved numerically, e.g., by employing a finite volume method (FVM), owing to its high-dimensionality (3+ dimensions of composition vector) the required computational effort would be tremendous. Alternatively, a Monte Carlo-based solution method can be employed-by generating a large number of flow realizations by evolving the model stochastic processes. In order to do this, we introduce the notion of computational particle, which represents a flow realization and carries properties such as phase, position, velocity, mobility, composition, density, mass, etc. As particles are transported through the computational domain (physical space), their properties evolve in the compositional space. Note that the particle statistics represent the statistics of the physical fluid volumes; the particle ensemble at a point represents the MDF at that location. Tyagi et al. (2008) developed the stochastic particle method (SPM) for simulating multi-phase flow in porous media, which is an extension of the particle method for single phase flows (Ahlstrom et al. 1977; Prickett et al. 1981; Kinzelbach 1992), and demonstrated its consistency and convergence. Below we list some important properties of the SPM that distinguish it from the other particle methods, which are mainly based on the method of characteristics (Dahle et al. 1990, 1995; Hewett and Yamada 1997):

- A particle belongs to a phase, i.e. in a simulation of n-phase flow, there are n-kinds of particles.
- Saturation is defined over an ensemble of particles and is not a particle property.
- A particle moves in physical space with a velocity such that the phase mass flux is equal to the conditional mass weighted expectation of the particle velocity times the particle mass density.
- Particle properties evolve in their respective sample spaces.

As a proof-of-concept, Tyagi et al. (2008) selected mobility as a particle property and modeled its evolution by a Langevin equation. The presence of finite correlation time in the mobility model gives rise to non-equilibrium fluxes that relax towards the equilibrium values at a rate equal to the inverse of the correlation time scale. Note that the SPM not only serves as a numerical method to solve MDF-equations but also provides a natural link between the Lagrangian evolution of the actual fluid volumes and the evolution of stochastic particles. Hence, stochastic models can easily be implemented into SPM codes.

[1] One should not confuse a grid cell with an REV when numerical simulation are performed within the PDF-framework.

It has to be mentioned here that being a particle-based stochastic method SPM is computationally expensive compared to standard Darcy based FVM implementations. For a detailed discussion on numerical and computational issues, interested readers are referred to our previous paper (Tyagi et al. 2008). SPM is not intended to solve those problems, where standard Eulerian FVM models give sufficiently accurate results. The potential of this new approach lies in modeling non-equilibrium phenomena and unstable scenarios. Moreover, based on SPM simulations one can derive closure models for the otherwise unclosed moment transport equations. Finally, these closed Eulerian moment equations can be implemented in standard FVM based simulators.

One of the possible applications of the PDF-approach is the modeling of density-driven countercurrent flow, which results as a consequence of the dissolution of one phase into other in a two-phase flow. Such density-driven flows play a crucial role during the post-injection phase of CO_2 storage in brine aquifers (Bachu 2003). After the injection of supercritical CO_2 at the bottom of a brine aquifer, the CO_2 plume migrates upwards due to buoyancy and slowly dissolves into the surrounding brine. The CO_2-rich brine is denser than the pure brine; consequently, the former sinks down and the latter rises up. Thus, the convective currents continuously bring fresh brine close to the dissolving CO_2 phase (Pruess and Garcia 2002; Riaz et al. 2006). To model this scenario within the PDF-approach, we consider particles representing CO_2 and brine phases, where each particle represents a physical fluid mass. Dissolution is modeled by exchanging mass among CO_2 and brine particles; a brine particle receives mass (at a certain rate) from the neighboring CO_2 particles till the concentration of dissolved CO_2 in it reaches the equilibrium concentration. As a brine particle gains some CO_2, it becomes denser compared to the pure brine particle; therefore, it sinks down. Accordingly, the lighter brine particles move up to fulfill the continuity requirement. The resulting particle movement indeed mimics the dynamics of countercurrent flow (fingers) due to the density gradient. The dependence of dissolved CO_2 concentration on brine particle vertical velocity, which in turn influences the transport of CO_2 in the brine phase, actually makes the flow nonlinear.

The paper is organized as follows. In Sect. 2, a general Lagrangian stochastic framework, which is essentially an extension of our previous method for incompressible flows (Tyagi et al. 2008), for compressible multi-phase flows is presented. The extended framework considers particles with varying mass and volume (or density) and is suitable for modeling interfacial mass transfer and mixing. In Sect. 3, we model the Lagrangian particle dynamics and the dissolution process. In Sect. 4, the MDF for multiphase flow is introduced and the Fokker–Planck equation governing its evolution in physical and compositional spaces—the MDF-equation—is derived. Furthermore, it is shown how this MDF-equation can be used to derive Eulerian equations for stochastic moments. Section 5 describes the simplifying assumptions used for the numerical simulation. In Sect. 6, some one- and two-dimensional numerical simulation results are presented. Finally, conclusions are drawn in Sect. 7.

2 Stochastic Particle Framework

Flow in porous media can be regarded as the irregular motion of infinitesimal fluid volumes, which may or may not be physically connected in the pore space. If an ensemble of large number of independent realizations of such a flow is considered, the irregular motion of infinitesimal fluid volumes can be modeled by randomly moving stochastic particles. The joint flow statistics is contained among the particles, whose properties as random variables evolve according to specified stochastic rules. For example, a simple, yet quite general stochastic rule for particle displacement in physical space is

$$\mathrm{d}X(t) = U(t)\mathrm{d}t + \sqrt{2\Gamma|U(t)|}\mathrm{d}W(t), \tag{2}$$

where $X(t)$ is the particle position, $U(t)$ the particle velocity, Γ a constant, and $W(t)$ a Wiener process with $\mathrm{d}W(t) = W(t+\mathrm{d}t) - W(t)$, $\langle \mathrm{d}W_i \rangle = 0$, $\langle \mathrm{d}W_i W_j \rangle = \delta_{ij}\mathrm{d}t$. Here δ_{ij} is the Kronecker delta, which is equal to 1 if $i = j$ and 0 otherwise. On the right hand side in Eq. 2, while the first term accounts for the displacement due to the instantaneous particle velocity, the second term models the pore scale dispersion with a dispersion coefficient proportional to the magnitude of instantaneous particle velocity. In its current form, however, Eq. 2 is unclosed and requires a model for particle velocity; this will be described in Sect. 3. Particles may carry additional flow properties and let all the relevant particle properties be contained in the composition vector $\boldsymbol{\Psi}$. Here, a set of Lagrangian equations of the form.[2]

$$\mathrm{d}\boldsymbol{\Psi}(t) = \boldsymbol{\alpha}\mathrm{d}t + \sqrt{\boldsymbol{\beta}}\mathrm{d}\boldsymbol{W}(t), \tag{3}$$

where the vectors coefficients $\boldsymbol{\alpha}$ and $\boldsymbol{\beta}$ are functions of $\boldsymbol{\Psi}$, is considered. Equation 3 is normally characterized by the correlation times and the variances, which can be, for instance, obtained from micro-scale studies.

In SPM, saturation is defined as an average quantity over an ensemble of particles (Tyagi et al. 2008). If fluid densities vary spatially, in addition to saturation, one also needs to define mean phase density. Let M, V, and ρ $(= M/V)$ be the particle mass, volume, and density, respectively. Then, the saturation, S_a, and the mean phase density, ρ_a, of phase a are defined by

$$S_\alpha = \frac{\langle V\delta_{Aa}\rangle}{\langle V\rangle} \quad \text{and} \quad \rho_a = \frac{\langle M\delta_{Aa}\rangle}{\langle V\delta_{Aa}\rangle} = \frac{\langle \rho V\delta_{Aa}\rangle}{\langle V\delta_{Aa}\rangle}, \tag{4}$$

where the random variable $A \in \{1, 2 \ldots n\}$ indicates the phase represented by the particle and δ_{Aa} is the Kronecker delta. The operator $\langle\cdot\rangle$ represents ensemble averaging and is defined by

$$\langle\cdot\rangle = \lim_{N_p\to\infty} \frac{1}{N_p} \sum_{i=1}^{i=N_p}. \tag{5}$$

Combining the two expressions in Eq. 4 gives

$$\langle M\delta_{Aa}\rangle = \rho_a S_a \langle V\rangle. \tag{6}$$

In order to be consistent with the definitions of mean phase density and saturation, mass weighted averaging (also known as Favre averaging) must be employed. The Favre average of a random variable Ψ conditioned on $A = a$ is defined by

$$\overline{\Psi|a} = \frac{\langle M\delta_{Aa}\Psi\rangle}{\langle M\delta_{Aa}\rangle} = \frac{\langle M\Psi|a\rangle}{\langle M|a\rangle}, \tag{7}$$

where the operator $\overline{\cdot}$ represents Favre averaging. Mass weighted averaging is indeed a natural choice while dealing with non-constant density flow; this fact will become apparent from the mean moment transport equations presented later in Sect. 4.

3 Stochastic Models

Here, we describe the particle velocity evolution and develop a particle model for interfacial mass transfer for a system of two phases (denoted by $a = 1$ and $a = 2$). While the

[2] In this paper, only continuous stochastic processes are considered.

phase-1 (CO_2 phase) always remains in its pure state, its only component (component-1, i.e. CO_2) dissolves into phase-2 (brine phase). The phase-1 density is constant and the density of phase-2 weakly depends on the concentration of component-1.

3.1 Particle Velocity

A model for particle velocity has to mimic the micro-scale physics of unstable density-driven flow. Dissolution leads to fine-scale variations of the phase-2 density, i.e. the density ρ of a phase-2 particle varies as a function of component-1 concentration; consequently, buoyancy forces within phase-2 are introduced. If it is assumed that particle mobility depends only on saturation and that fine-scale pressure fluctuations are negligible, the particle velocity, U, can be expressed as

$$U = -\frac{k_{\mathrm{r}_a} k}{\phi S_a \mu_a} (\nabla p_a + \rho g e_z) \tag{8}$$

for phase $a \in \{1, 2\}$. Furthermore, it is assumed that the density ρ of the phase-1 particles remains constant, i.e. $\rho = \rho_1$ and that the phase pressures are related by the macroscopic capillary pressure relation

$$p_1 - p_2 = P_{\mathrm{c}}(S_2). \tag{9}$$

Note that the mean phase volume fluxes based on the rule (8) for $\Gamma = 0$ are

$$\begin{aligned} F_1 &= \phi S_1 \overline{U|a=1} = -\frac{k_{\mathrm{r}_1} k}{\mu_1} (\nabla p_1 + \rho_1 g e_z) \quad \text{and} \\ F_2 &= \phi S_2 \overline{U|a=2} = -\frac{k_{\mathrm{r}_2} k}{\mu_2} \left(\nabla p_2 + \overline{\rho|a=2}\, g e_z\right), \end{aligned} \tag{10}$$

which are consistent with classical two-phase Darcy formulations. Although more general rules can be derived, however, since the focus of this paper is to demonstrate the concept, the particle velocity model (8) will be used.

3.2 Dissolution and Mixing

We consider mass transfer from phase-1 particles to phase-2 particles with finite rate kinetics. For this purpose a concentration, C, of component-1, which is defined as

$$C = \frac{M_{\mathrm{c}}}{M}, \tag{11}$$

where M_{c} is the mass of component-1 carried by the particle, is introduced. Note that since phase-1 always remains in the pure state, $C = 1$ for all phase-1 particles. To model dissolution a particle ensemble with spatial ergodicity is considered, in which during an infinitesimal time interval, first the mass of all phase-2 particles is evolved according to a linear relaxation equation, and then the mass of the phase-1 particles is consistently computed to guarantee mass balance of all components.

3.2.1 Phase-2 Particles

Concentration of a phase-2 particle can be altered either by mass transfer from the phase-1 particles (dissolution) or by mass exchange with the other phase-2 particles (molecular

mixing). Dissolution is modeled by a first order rate law

$$r_{\mathrm{d}} = -\frac{M}{\tau_{\mathrm{d}}}(C - C^{\mathrm{eq}}), \tag{12}$$

where τ_{d} is the characteristic dissolution time and C^{eq} the equilibrium concentration of component-1 in phase-2. The molecular mixing rate of component-1 in phase-2 is modeled by a concentration drift towards the conditional Favre mean concentration $\overline{C|a=2}$, i.e.

$$r_{\mathrm{m}} = -\frac{M}{\tau_{\mathrm{m}}}(C - \overline{C|a=2}), \tag{13}$$

where τ_{m} is the characteristic mixing time. Combining Eqs. 12 and 13 gives the evolution

$$\frac{\mathrm{d}M}{\mathrm{d}t} = -\frac{M}{\tau_{\mathrm{d}}}(C - C^{\mathrm{eq}}) - \frac{M}{\tau_{\mathrm{m}}}(C - \overline{C|a=2}) \tag{14}$$

for the phase-2 particle mass. Since the brine mass of a phase-2 particle does not change, the following mass balance must hold

$$\frac{\mathrm{d}M}{\mathrm{d}t} = \frac{\mathrm{d}(MC)}{\mathrm{d}t}, \tag{15}$$

which leads to

$$\frac{1}{M}\frac{\mathrm{d}M}{\mathrm{d}t} = \frac{1}{1-C}\frac{\mathrm{d}C}{\mathrm{d}t}. \tag{16}$$

After the substitution of Eq. 16 into Eq. 14, the evolution equation

$$\frac{1}{1-C}\frac{\mathrm{d}C}{\mathrm{d}t} = -\frac{1}{\tau_{\mathrm{d}}}(C - C^{\mathrm{eq}}) - \frac{1}{\tau_{\mathrm{m}}}(C - \overline{C|a=2}) \tag{17}$$

for component-1 concentration in a phase-2 particle is obtained.

3.2.2 Phase-1 Particles

In an ensemble, the mass gained by phase-2 particles must be equal to the mass lost by phase-1 particles, i.e.

$$\left\langle \delta_{A1}\frac{\mathrm{d}M}{\mathrm{d}t}\right\rangle = -\left\langle \delta_{A2}\frac{\mathrm{d}M}{\mathrm{d}t}\right\rangle \tag{18}$$

In order to distribute the lost mass among the individual phase-1 particles, it is assumed that a phase-1 particle in the ensemble looses mass at a rate proportional to its own mass, i.e.

$$\frac{\mathrm{d}M}{\mathrm{d}t} = -\frac{M}{\langle M\delta_{A1}\rangle}\left\langle \delta_{A2}\frac{\mathrm{d}M}{\mathrm{d}t}\right\rangle. \tag{19}$$

Substituting for $\langle \delta_{A2}\mathrm{d}M/\mathrm{d}t\rangle$ using Eq. 14 gives the mass evolution

$$\frac{\mathrm{d}M}{\mathrm{d}t} = M\frac{\langle M\delta_{A2}\rangle}{\langle M\delta_{A1}\rangle}\frac{(\overline{C|a=2} - C^{\mathrm{eq}})}{\tau_{\mathrm{d}}} \tag{20}$$

for a phase-1 particle. Further, with $\langle M\delta_{A2}\rangle/\langle M\delta_{A1}\rangle = (\rho_2 S_2)/(\rho_1 S_1)$ from Eq. 6 one can rewrite Eq. 20

$$\frac{\mathrm{d}M}{\mathrm{d}t} = M\frac{\rho_2 S_2}{\rho_1 S_1}\frac{(\overline{C|a=2} - C^{\mathrm{eq}})}{\tau_{\mathrm{d}}} \tag{21}$$

for a phase-1 particle.

The dissolution time, τ_d, introduced above would require further modeling. In general, τ_d itself could be a random quantity that would evolve according to some stochastic process. In the present paper, however, we limit ourselves to a simple model, which is sufficient to demonstrate the concept, for τ_d. This model is based on the physics that in an ensemble, the average mass transfer rate to a phase-2 particle depends on the probability of finding phase-1 particles. Assuming this dependency follows a linear relationship, one can write

$$\frac{1}{\tau_d} = \frac{S_1}{\tau_0}, \tag{22}$$

where τ_0 is the dissolution time in the limit of unit phase-1 saturation ($S_1 \to 1$). This relationship is in the agreement with the fact that when $S_1 = 0$, the dissolution ceases as there is no more phase-1 to dissolve.

3.3 Particle Densities

Dissolution and mixing alter the phase-2 particle mass and volume; hence the phase-2 particle density. A complete closure of the problem would require the relations connecting phase densities with other thermodynamics variables. In this paper, it is assumed that the phase-2 particle density is a linear function of component-1 concentration (Riaz et al. 2006). Thus, the density of a particle can be expressed as

$$\rho = \rho_a^0 + \delta_{a2}\frac{(\rho_2^{\text{eq}} - \rho_2)}{C^{\text{eq}}}C, \quad a \in \{1, 2\} \tag{23}$$

where ρ_1^0 and ρ_2^0 are the phase densities in the pure states and ρ_2^{eq} is the equilibrium density (corresponding to $C = C^{\text{eq}}$ in phase-2). Note that the phase-1 density remains constant-an approximation that is valid in Boussinesq limit (shown later).

4 MDF-Equation

In this section, we show how the particle properties evolutions described before lead to transporting a MDF in physical and compositional spaces. This equivalence between the particle evolution and the MDF evolution is widely used in many fields of science and engineering, for example, in modeling turbulent reactive flows (Pope 1985; Heinz 2003). If $f^a(c; x, t)$ is the mass weighted conditional PDF of C for phase a, the MDF of the entire multi-phase system can be expressed as $\mathcal{F}(a, c, x; t) = \phi\rho_a(x, t)S_a(x, t)f^a(c; x, t)$. By definition, $\mathcal{F}(a, c, x; t)\mathrm{d}x\mathrm{d}c$ is the mass of phase-a in an infinitesimal volume $\mathrm{d}x\mathrm{d}c$ in $x - c$ space at time t. Any stochastic moment of C can be obtained once the MDF is known:

$$\int_{\mathbb{R}^2} c^n \mathcal{F}(c, a, x; t)\mathrm{d}c = \phi\rho_a(x, t)S_a(x, t)\overline{C^n|a}\,(x, t), \quad n \in \{0, 1, 2\ldots\}, \tag{24}$$

where $\overline{C^n|a}$ is the nth conditional mass weighted moment of C. As shown in Appendix, a transport equation for $\mathcal{F}$ can be derived by balancing mass in $\boldsymbol{x} - c - a$ space. For the present

case, this is

$$\begin{aligned}
&\frac{\partial \mathcal{F}}{\partial t} + \nabla \cdot \left\{ \left(-\frac{k_{r_1} k}{S_1 \phi \mu_1} (\nabla p_1 + \rho_1 g e_z) \delta_{a1} - \frac{k_{r_2} k}{S_2 \phi \mu_2} (\nabla p_2 + \rho g e_z) \delta_{a2} \right) \mathcal{F} \right\} \\
&\quad + \frac{\partial}{\partial c} \left\{ \left(-\frac{(1-c)(c - C^{\mathrm{eq}}) \delta_{a2}}{\tau_{\mathrm{d}}} - \frac{(1-c)(c - \overline{C|a=2}) \delta_{a2}}{\tau_{\mathrm{m}}} \right) \mathcal{F} \right\} \\
&= \left\{ -\frac{\delta_{a2}(c - C^{\mathrm{eq}})}{\tau_{\mathrm{d}}} - \frac{\delta_{a2}(c - \overline{C|a=2})}{\tau_{\mathrm{m}}} + \frac{\delta_{a1} \rho_2 S_2}{\rho_1 S_1} \frac{(\overline{C|a=2} - C^{\mathrm{eq}})}{\tau_{\mathrm{d}}} \right\} \mathcal{F} \\
&\quad + \nabla^2 \left\{ \langle \Gamma | U | | x, a, c; t \rangle \, \mathcal{F} \right\}, \qquad (25)
\end{aligned}$$

which is a Fokker–Planck equation (with source term) describing the evolution of the MDF in $x - c - a$ space.

4.1 Moment Equations and Closure Problem

Equation 25 can be used to derive Eulerian transport equations for expectations, variances, and other stochastic moments. For example, the integration of Eq. 25 over the entire c-space yields the saturation equations

$$\begin{aligned}
\frac{\partial(\phi \rho_1 S_1)}{\partial t} - \nabla \cdot \left\{ \frac{\rho_1 k_{r_1} k}{\mu_1} (\nabla p_1 + \rho_1 g e_z) \right\} &= \nabla^2 \left\{ \phi \rho_1 S_1 \overline{\Gamma | U | | a = 1} \right\} \\
&\quad + \phi \rho_2 S_2 \frac{(\overline{C|a=2} - C^{\mathrm{eq}})}{\tau_{\mathrm{d}}} \qquad (26)
\end{aligned}$$

for $a = 1$ and

$$\begin{aligned}
\frac{\partial(\phi \rho_2 S_2)}{\partial t} - \nabla \cdot \left\{ \frac{\rho_2 k_{r_2} k}{\mu_2} \left(\nabla p_2 + \overline{\rho | a=2} \, g e_z \right) \right\} &= \nabla^2 \left\{ \phi \rho_2 S_2 \overline{\Gamma | U | | a = 2} \right\} \\
- \phi \rho_2 S_2 \frac{(\overline{C|a=2} - C^{\mathrm{eq}})}{\tau_{\mathrm{d}}} \qquad (27)
\end{aligned}$$

for $a = 2$. An equation for conditional Favre mean concentration can be obtained by multiplying Eq. 25 at $a = 2$ by c, and subsequently integrating over the entire c-space:

$$\begin{aligned}
&\frac{\partial(\phi \rho_2 S_2 \overline{C|a=2})}{\partial t} - \nabla \cdot \left\{ \frac{\rho_2 k_{r_2} k}{\mu_2} \left(\nabla p_2 \overline{C|a=2} + \overline{\rho C | a=2} g e_z \right) \right\} \\
&\quad = \nabla^2 \left\{ \phi \rho_2 S_2 \overline{\Gamma (|U|C) | a=2} \right\} - \frac{\phi \rho_2 S_2 (\overline{C|a=2} - C^{\mathrm{eq}})}{\tau_{\mathrm{d}}}. \qquad (28)
\end{aligned}$$

As ρ is a function of C, it is evident that even if only the mean quantities are of interest, Eqs. 26–28 are not sufficient to determine them, since $\overline{\rho C | a=2}$ is not closed in the second term on the left hand side of Eq. 28. Indeed, it can be shown that a system of equations derived from Eq. 25 for the first n-moments would have at least $n + 1$ unknowns. Thus, an Eulerian approach with a system of finite moment equations is subjected to closure problems, which do not arise in the PDF-approach. In the classical Darcy-approach, dissolution process is modeled using only mean quantities, i.e. the approximation

$$\overline{C^2 | a=2} = \overline{C|a=2}^2 \qquad (29)$$

is made in Eq. 28; thus, the influence of higher stochastic moments is neglected.

5 Boussinesq Flow

In many scenarios, one can greatly simplify the full compressible flow model by making a Boussinesq approximation, which implies that density variations are only important in the gravity term; otherwise,

$$\rho_2 = \text{constant} \tag{30}$$

is used. Here, we further simplify the problem by assuming

$$\rho_1 = \rho_2 = \text{constant} \tag{31}$$

everywhere except in the gravity term. Moreover, any macroscopic capillary pressure effect is ignored, i.e. P_c is set to zero in Eq. 9 leading to $p_1 = p_2 = p$.

5.1 Pressure Equation

With the assumption (31) and the relation (9) the summation of Eqs. 26 and 27 leads to the elliptic equation

$$\begin{aligned} -\nabla \cdot \{k\lambda \nabla p\} = g e_z \cdot \nabla \left\{k\lambda_1 \rho_1 + k\lambda_2 \overline{\rho | a=2}\right\} \\ +\nabla^2 \left\{\phi \left(S_1 \overline{\Gamma | U || a=1} + S_2 \overline{\Gamma | U || a=2}\right)\right\}, \end{aligned} \tag{32}$$

for the pressure p, where $\lambda_1 = k_{r_1}/\mu_1$ and $\lambda_2 = k_{r_1}/\mu_2$ are the mobilities of phase-1 and phase-2, respectively, and $\lambda = \lambda_1 + \lambda_2$ is the total mobility.

5.2 Fractional Flow Formulation

Form Eq. 32 we can define a total volume flux

$$\begin{aligned} F = -k\lambda \nabla p - k\left(\lambda_1 \rho_1 + \lambda_2 \overline{\rho | a=2}\right) g e_z \\ -\nabla \left\{\phi \left(S_1 \overline{\Gamma | U || a=1} + S_2 \overline{\Gamma | U || a=2}\right)\right\} \end{aligned} \tag{33}$$

that fulfills the conservation law

$$\nabla \cdot F = 0. \tag{34}$$

The particle velocities are expressed in fractional flow formulation:

$$U = \begin{cases} \frac{1}{\phi S_1 \lambda}\left[\lambda_1 F + k\lambda_1\lambda_2(\overline{\rho | a=2} - \rho_1) g e_z + \lambda_1 \nabla\{\phi(S_1 \overline{\Gamma | U || a=1} \right. \\ \quad \left. + S_2 \overline{\Gamma | U || a=2})\}\right], \quad \text{if } a = 1, \\ \\ \frac{1}{\phi S_2 \lambda}\left[\lambda_2 F + k\lambda_1\lambda_2(\rho_1 - \rho) g e_z - k\lambda_2^2(\rho - \overline{\rho | a=2}) g e_z \right. \\ \quad \left. + \lambda_2 \nabla\{\phi(S_1 \overline{\Gamma | U || a=1} + S_2 \overline{\Gamma | U || a=2})\}\right], \quad \text{if } a = 2, \end{cases} \tag{35}$$

which are obtained by eliminating the pressure gradient in Eq. 8 using Eq. 33.

5.3 Multi-Phase Flow Parameters and Important Scales

For numerical simulations, quadratic relative permeabilities, i.e.

$$k_{r_1} = S_1^2 \quad \text{and} \quad k_{r_2} = S_2^2 \tag{36}$$

are chosen. Note that in principle, any general shape of relative permeability–saturation curves can be employed, however, since the choice of a specific relative permeability curve

would not alter the concept, which is the focus of this paper, simulations are performed only using Eq. 36. Molecular mixing is assumed to be a very slow process compared to dissolution and convection; therefore, it is neglected here.

Note that, in the present case, there exist two kind of buoyant forces: one due to the phase density difference, $\rho_2 - \rho_1$ and the other due to the density fluctuations within phase-2. An estimate for the average buoyancy induced phase-2 velocity is

$$U_g = \frac{kg(\rho_2 - \rho_1)}{\mu_2 \phi}. \tag{37}$$

If H is chosen as the characteristic height of the problem, the time scale

$$\tau_g = \frac{\mu_2 \phi H}{kg(\rho_2 - \rho_1)} \tag{38}$$

can be associated to the downward motion of phase-2. In similar way, an estimate for the average buoyancy induced velocity within phase-2 is

$$U_\rho = \frac{kg\left(\rho_2^{\text{eq}} - \rho_2\right)}{\mu_2 \phi}, \tag{39}$$

which leads to the time scale

$$\tau_\rho = \frac{\mu_2 \phi H}{kg\left(\rho_2^{\text{eq}} - \rho_2\right)} \tag{40}$$

for the density-driven currents within phase-2. The relative importance of the two buoyancy mechanisms can be estimated by the ratio $\tau_g/\tau_\rho = \left(\rho_2^{\text{eq}} - \rho_2\right)/(\rho_2 - \rho_1)$.

6 Numerical Simulation Results

Here, some one- and two-dimensional results with the focus on demonstrating differences between PDF and Darcy modeling approaches are presented. In the PDF-approach, SPM is employed, i.e. the computational particles are moved in the computational domain using Eq. 2, where the velocities are given by (35), and their properties are evolved according Eqs. 14, 17, and 21. The pressure equation (32) is solved on an FVM grid at every time step to obtain the total volume flux (33), which is then used to compute the particle velocities (35). In the Darcy-approach, one could solve the mean Eqs. 26–28 together with the closure assumption (29) by employing FVM. However, in order to avoid numerical discrepancy due to different solution methods, and since the goal here is to demonstrate differences between the two approaches, an FVM-based implementation in the Darcy-approach is avoided. Instead, the same is achieved by decorrelating the particle properties, i.e. ρ in Eq. 35 is replaced by $\overline{\rho|a=2}$ in SPM simulations. This would be equivalent to having a closed set of equations for saturations and mean concentration. The Boussinesq approximation as described in Sect. 5 is made in both cases. Since the focus of this paper is the modeling aspect of the PDF-approach, numerical and computational details/issues related to particle tracking, pressure-transport coupling, interpolation schemes, accuracy, etc. are not given here. Interested readers may refer to the numerical schemes those presented in Tyagi et al. (2008), Jenny et al. (2001), Rembold and Jenny (2006). The simulation test cases are constructed by idealizing the dynamics observed during the post-injection phase of CO_2 storage. After the injection of CO_2 near the bottom of saline aquifer, a plume of lighter CO_2 (phase-1) migrates upwards in the aquifer, which is otherwise filled with the denser brine (phase-2). As the

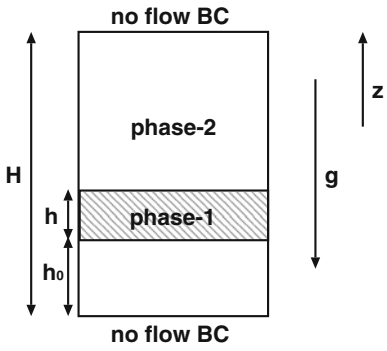

Fig. 1 Geometry and initial distribution of phases in the 1D test case

plume rises, some CO_2 dissolves into the surrounding brine phase leading to local increase in the brine density. This density stratification drives additional gravity currents within the brine phase.

It has to be emphasized that the model presented in this paper comprises several paramaters, which control the flow dynamics. A detailed investigation of the flow dynamics in the entire parameter space would be impossible to cover in a single paper. Moreover, the goal here is to demonstrate the concept but to present a systematic parametric study. Therefore, for all simulations, $C^{\text{eq}} = 0.1$ is chosen in the dissolution model and both the parameters τ_g/τ_ρ and the viscosity ratio μ_2/μ_1 are equal to one. A unity value of τ_g/τ_ρ means that the upward migration of CO_2 and the density-driven currents in brine have the same time scale. A unity value of μ_2/μ_1 insures that there is no viscous instability, presence of which would further complicate the flow physics.

6.1 One-Dimensional Numerical Results

First, a one-dimensional (1D) test case, which represents a simple model of rising CO_2 plume in brine aquifer, is considered. The geometrical details and initial distribution of phases are shown in Fig. 1, where $h_0 = 0.1H$ and $h = 0.2H$. At $t = 0$, particles of equal mass and volume such that $A = 1$ and $C = 1$, if $0.1H \leq z \leq 0.3H$ and $A = 2$ and $C = 0$ elsewhere, are uniformly distributed in the domain. Total volume flux is zero at boundaries implying $F_z = 0$ everywhere. The gravitational acceleration is directed along the decreasing z-axis. A grid with 100 equally spaced finite volumes (grid cells), i.e. $\Delta z = 0.01H$, is employed to discretize the domain and a time step size of $\Delta t = 5 \times 10^{-3}\tau_g$ is used during the simulations (the maximum CFL[3] number in the domain is less than 0.5). In order to obtain smooth stochastic moments, an average of 50,000 particles per cell are employed.

Figure 2a, b depicts a comparison of the spatial phase-2 saturation profiles at $t = \tau_g$ and $t = 2\tau_g$, respectively, obtained with the PDF and Darcy approaches for $\tau_0 = 0.1\tau_g$. The difference between the saturations from the two approaches is negligible; thus, for the present test case the Darcy-approach provides a sufficiently accurate description of the average phase distribution. Figure 3a, b depicts the corresponding spatial profiles for the conditional Favre mean concentration $\overline{C|a=2}$. In the trailing region of the plume, a significant difference between the mean concentrations obtained from the two approaches can be observed. The non-monotonic mean concentration profile predicted by the PDF-approach is due to unstable density-driven countercurrents in the phase-2. In the PDF-approach, this phenomenon

[3] If $|U|$ is the magnitude of particle velocity, the CFL number is defined as $\frac{|U|\Delta t}{\min\{\Delta x_i\}}$.

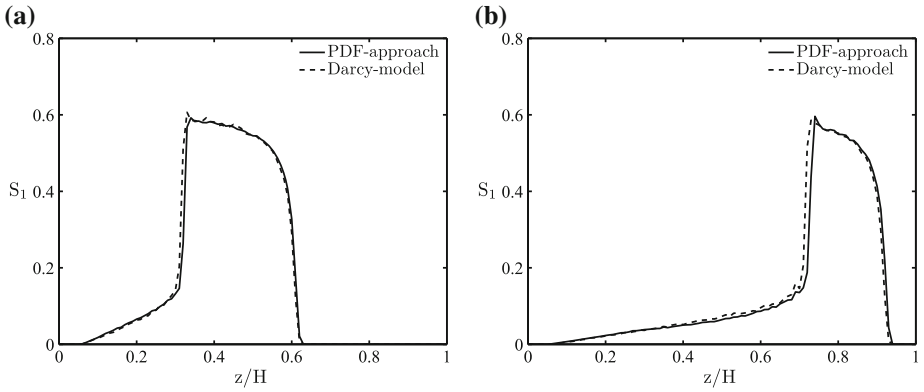

Fig. 2 Phase-1 saturation profiles obtained with the PDF-approach and the Darcy-model for $\tau_0 = 0.1\tau_g$ at: **a** $t = \tau_g$; **b** $t = 2\tau_g$

is modeled by the stochastic formulation of phase-2 particle velocities (see Eq. 35), i.e. the term

$$-\frac{k\lambda_2^2(\rho - \overline{\rho|a=2})ge_z}{S_2\phi\lambda}, \tag{41}$$

which is absent in the Darcy model (see Sect. 4). According to this term, in phase-2, a particle with higher density than the local mean density sinks and a particle with lower density than the local mean density rises. Thus, density-driven countercurrent miscible flow is very naturally mimicked by the movement of particles. In a one-dimensional Darcy-modeling framework, these unstable miscible currents, which have their origin at the micro-scale, cannot be accounted. It should be noted, however, that if one performs a well-resolved two- (or three-) dimensional simulation with Darcy's model, it is possible to capture these unstable miscible currents as gravity fingers. However, such a fine-scale simulation would demand tremendous computational resources, and thereby is not suited for most subsurface flows. The PDF-approach, on the other hand, provides a computationally inexpensive way to capture such phenomena; the average flow field can be described without resolving the finest scale. In the present example, this could, for instance, imply averaging of a two- $(x - z)$ or three- $(x - y - z)$ dimensional flow on the vertical line (z-axis).

Statistically, the magnitude of countercurrent flow can be measured by the concentration variance ($\sigma^2 = \overline{C^2|a=2} - \overline{C|a=2}^2$). Figure 4a, b depicts the time evolutions of σ for $\tau_0 = 0.1\tau_g$ and $\tau_0 = \tau_g$, respectively. Variance, in general, is larger where (and when) the mean concentration profile has a dip (Fig. 3a, b). Indeed, variance, which represents the unstable countercurrent flow, drives the transport of mean concentration in the PDF-approach. This, however, is not the case with the Darcy's approach, which neglects variance.

At any point on z-axis, the concentration distribution (PDF) estimated over a particle ensemble represents the concentration variation due to fine scale countercurrent flows. Figure 5 depicts the time evolution of the mass weighted conditional PDF of $C - \overline{C|a=2}$ at $x = 0.5H$. Its shape changes form uni-modal to bi-modal and then changes back to uni-modal. At early times, the component-1 concentration of the phase-2 particles increases due to dissolution; therefore, the PDF is uni-modal. Meanwhile, also due to dissolution, the phase-2 particles become denser and begin to sink. To satisfy mass conservation, the lighter phase-2 particles rise; this leads to a bi-modal PDF, where one mode represents the denser

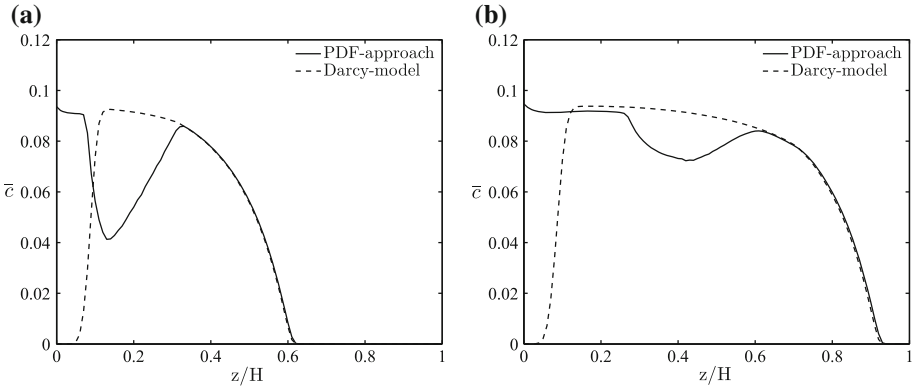

Fig. 3 Favre mean component-1 concentration in phase-2 obtained with the PDF-approach and the Darcy-model for $\tau_0 = 0.1\tau_g$ at: **a** $t = \tau_g$; **b** $t = 2\tau_g$

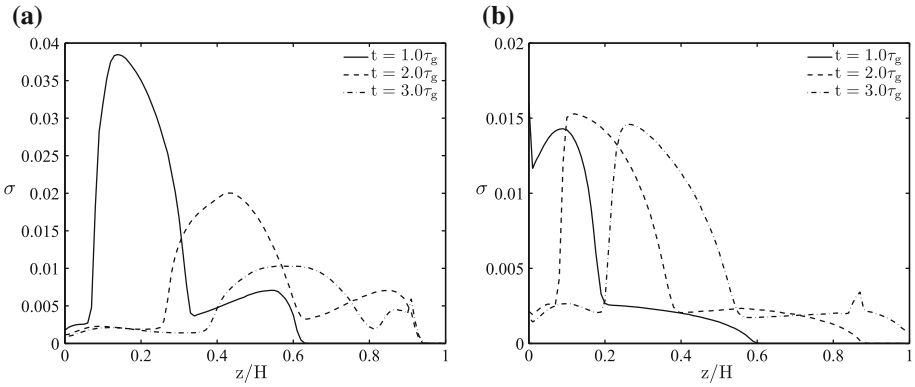

Fig. 4 Standard deviation (σ) of component-1 concentration in phase-2 at three different times for: **a** $\tau_0 = 0.1\tau_g$; **b** $\tau_0 = \tau_g$

particles and the other one the lighter particles. The bi-modal shape of the PDF is essentially due to the countercurrent miscible flow; the denser particles sink and the lighter particles rise. At later times, the initially lighter particles eventually gain enough component-1 mass leading again to a uni-modal PDF. The non-monotonic mean concentration profiles shown in Fig. 3a, b are actually due to the bi-modal shape of the PDF. Thus, we notice that the details of complex PDF-evolutions strongly determine the mean concentration distribution; this is indeed the best motivation for using PDF-approach.

6.2 Two-Dimensional Numerical Results

Although the basic differences between the PDF and Darcy approaches are clear from the 1D results presented above, more interesting cases involve two and three spatial dimensions. For this purpose, a two-dimensional (2D) simulation test case in which a plume of the lighter phase-1 rises upwards in a porous medium filled with the denser phase-2 is considered. The geometrical details and initial configuration of phases are shown in Fig. 6, where $l = 0.5L$, $h = 0.25H$, and $r = 0.2L$. At $t = 0$, particles of equal mass and volume such

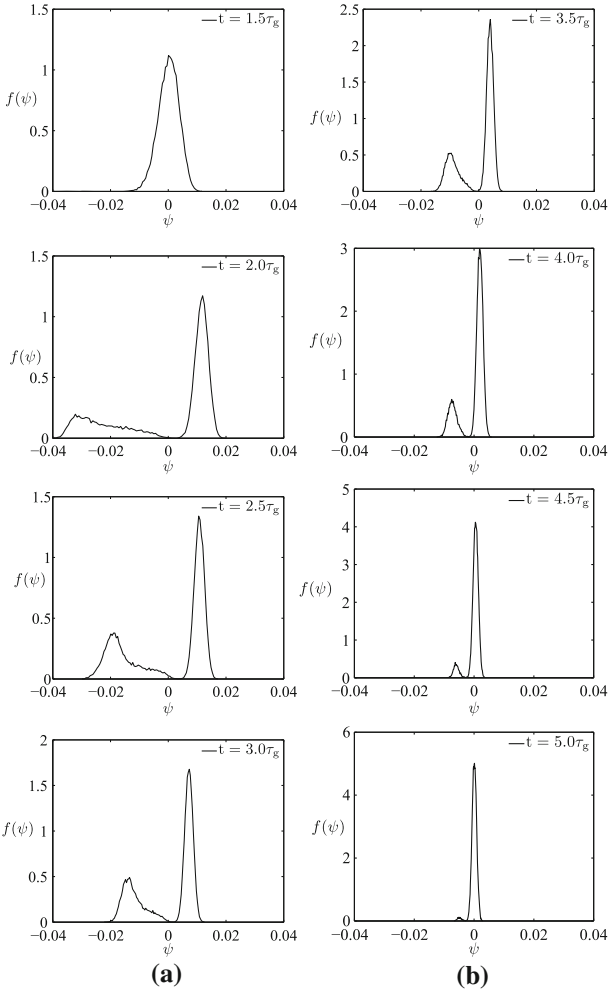

Fig. 5 Time evolution of the mass weighted conditional PDF $f(\psi)$ of fluctuating component-1 concentration in phase-2 at $z = 0.5H$ for $\tau_0 = 0.1\tau_g$, where $\psi = c - \overline{C|a=2}$

that $A = 1$ and $C = 1$, if $(x - l)^2 + (z - h)^2 \leq r^2$, and $A = 2$ and $C = 0$ elsewhere, are uniformly distributed in the domain. The domain is a square $(H/L = 1)$ homogeneous porous medium with no-flow conditions at all boundaries. A uniform orthogonal finite volume grid with 100×100 grid cells is employed to discretize the computational domain. The time step size is chosen such that CFL condition is satisfied everywhere. In order to obtain smooth stochastic moments, an average of 4,000 particles per cell are employed.

First, some results to show the general multi-phase flow dynamics are presented; $\tau_0 = 0.1\tau_g$ is chosen for the simulation. Figure 7 depicts the time evolution of the phase-1 particle distribution, where for the sake of clarity only a random subset of all particles is depicted. As the plume migrates upwards, a trail of phase-1 is left behind; this represents the imbibition expansion fan. Upon reaching the ceiling, the phase-1 particles begin to move laterally. Figure 8 depicts the corresponding time evolution of the total volume flux F, which is given

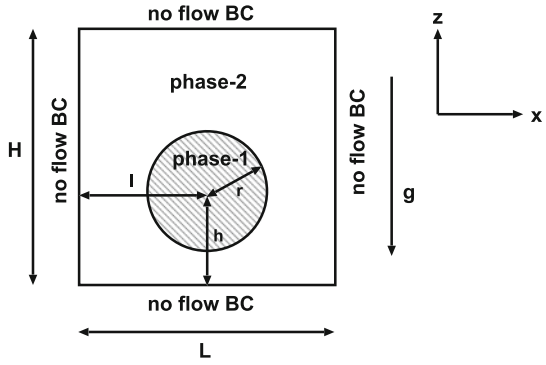

Fig. 6 Geometry and initial distribution of the phases in the 2D test case

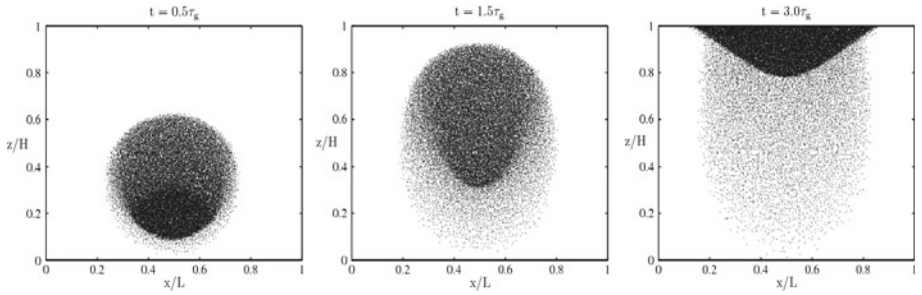

Fig. 7 Time evolution of phase-1 particles with $\tau_0 = 0.1\tau_g$. Only a fraction of all particles are shown

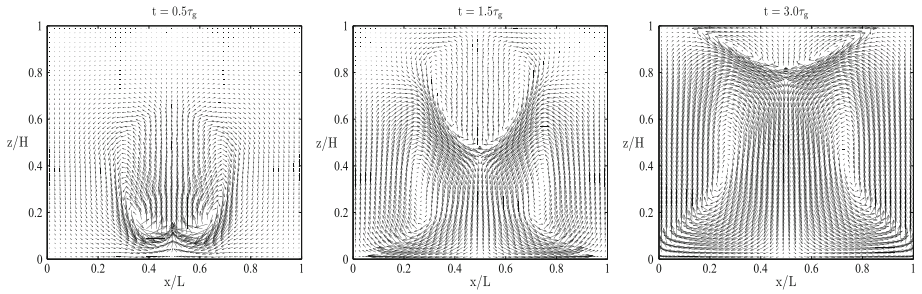

Fig. 8 Time evolution of the total volume flux vectors for $\tau_0 = 0.1\tau_g$

by Eq. 33. While the plume migrates upwards, phase-2 is entrained from the side leading to a prime recirculation. These recirculation zones are clearly visible at $t/\tau_g = 0.5$ and also, though weaker in strength, at later times. As the flow evolves, some mass from phase-1 dissolves into phase-2; consequently, the denser phase-2 particles sink (and the lighter rise) resulting in additional (density-driven) secondary recirculation zones, which grow in size with time.

Next, similar to the 1D case, a comparison between the results obtained from the two different modeling approaches is presented. Figure 9a, b depicts the total volume flux vectors at $t = 2\tau_g$ obtained from the PDF- and Darcy-approaches, respectively. A visible difference between the density-driven (secondary) recirculation zones can be clearly noticed. Note that the PDF-approach predicts more lateral convection in the trailing region. The difference in

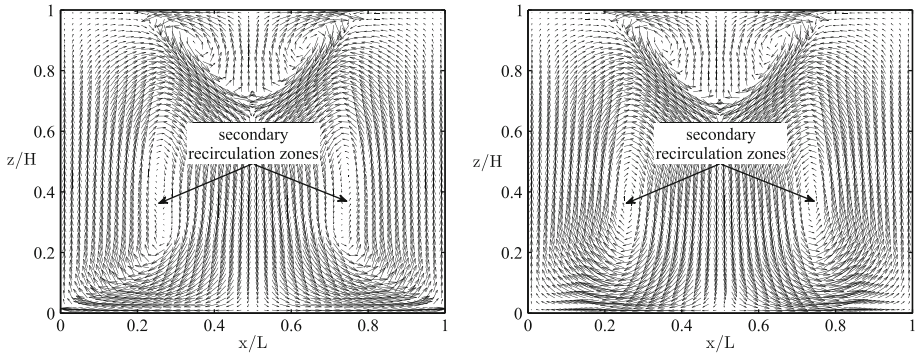

Fig. 9 Total volume flux vectors at $t = 2\tau_g$ for $\tau_0 = 0.1\tau_g$ obtained with: **a** the PDF-approach; **b** the Darcy-model

the results from the two approaches is even more pronounced in the concentration fields, which are shown in Fig. 10a, b obtained from the PDF- and Darcy-approaches, respectively. Here, the isolines of the Favre mean dissolved component-1 concentration are plotted at four different times. Note that the observed difference, which is primarily due to the stronger lateral convection as predicted by the PDF-approach, increases with time. The effect of convection on concentration field is clearly visible in the iso-concentration contours shown at $t = 2\tau_g$ as these counters align themselves with the secondary recirculation zones (see Fig. 9a, b). To further demonstrate the difference between the results obtained from the two approaches, phase-2 particle distributions with $C > 0.5C^{\text{eq}}$ at $t = 10\tau_g$ are shown in Fig. 11a, b. Again a drastic difference between the two particle distributions can be observed. Unlike the Darcy-approach the PDF-approach accounts for the influence of fine-scale countercurrent flow on large-scale dynamics. Therefore, the denser phase-2 particles in the simulation with the PDF-approach reach the bottom of the aquifer much quicker than that in the simulation with the Darcy-approach. For practical applications, one is often interested in knowing the total amount of CO_2 that has dissolved in brine as a function of time. This is shown in Fig. 12, where the dimensionless dissolved component-1 masses in phase-2 obtained with the PDF- and Darcy-approaches are plotted as functions of time. Opposed to the Darcy-simulation, in the PDF-simulation, due to density-driven enhanced advective transport, fresh phase-2 particles are continuously made available to phase-1 particles, thereby leading to a significantly higher dissolution rate.

7 Conclusions

Modeling of small-scale flow features is crucial for unstable porous media flows, if long range correlations, e.g., gravity or viscous fingers, are present. In order to obtain an accurate macroscopic flow description, large-scale flow models must account for such correlations. The PDF-approach provides a statistical framework to consistently model the influence of microscopic dynamics on macroscopic flow. In this paper, the PDF-approach is used to model dissolution (one-way), and the resulting unstable density-driven currents in two-phase flow through porous media. Mathematically, the modeling approach is described by a high dimensional MDF-equation in physical and concentration spaces. Using this equation it can be shown that irrespective of the number of moments considered, a system of

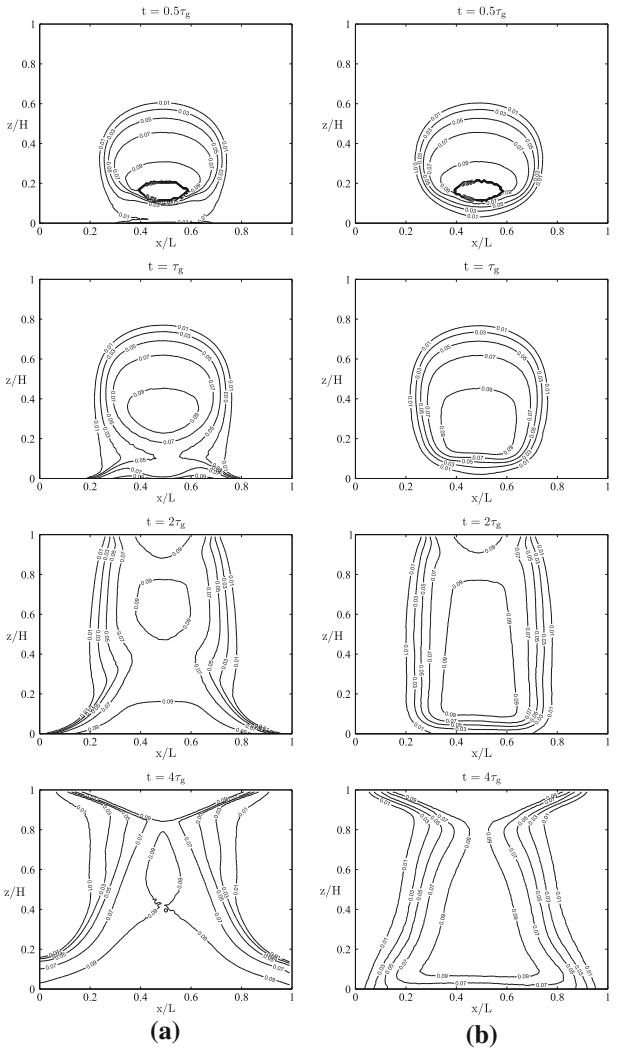

Fig. 10 Time evolution of the Favre mean concentration of component-1 in phase-2 for $\tau_0 = 0.1\tau_g$ obtained with: **a** the PDF-approach; **b** the Darcy-model

Eulerian equations for stochastic moments remains unclosed. In the Darcy-modeling approach, the effect of higher moments is ignored, i.e. flow and transport are completely described by average quantities. With several one- and two-dimensional simulations it is shown that the results, particularly the CO_2 concentration in brine phase, obtained with the PDF-approach significantly differ from those obtained with the Darcy-approach. However, for the test cases considered in this paper, the choice of simulation approach does not have a visible influence on saturation field. The density-driven countercurrents simulated with the two models are significantly different; this in turn, leads to drastic differences in the concentration distributions of dissolved CO_2 in brine. The reason for this difference is the

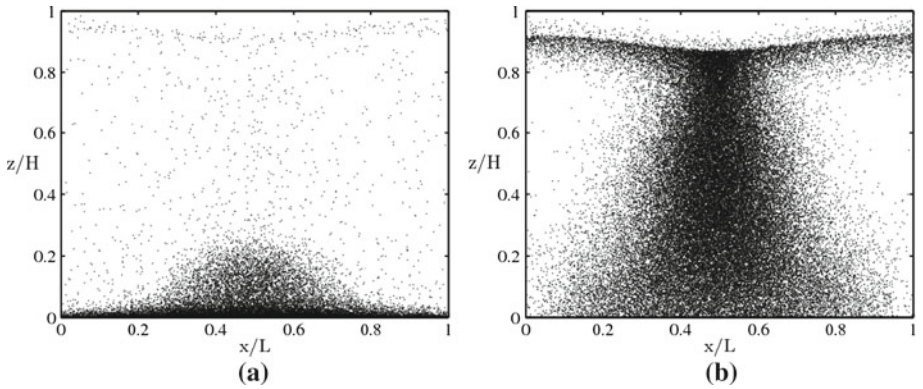

Fig. 11 Phase-2 particle distribution with $C > 0.5C^{\text{eq}}$ at $t = 10\tau_g$ for $\tau_0 = 0.1\tau_g$ obtained with: **a** the PDF-approach; **b** the Darcy-model. Only a fraction of all particles are shown

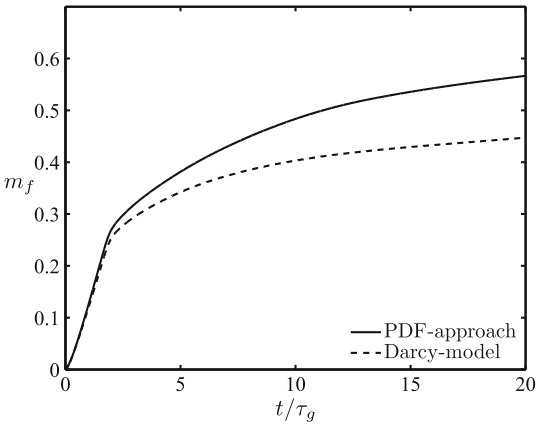

Fig. 12 Fraction of global component-1 mass in phase-2 as function of dimensionless time for $\tau_0 = 0.1\tau_g$

lack of information about the microscopic density-driven dynamics in the Darcy-model. This information, on the other hand, is very naturally captured in the PDF-approach.

Acknowledgments The authors wish to acknowledge Prof. Hamdi A Tchelepi, Stanford University with whom they had many useful discussions. This research was supported by the Global Climate and Energy Project at Stanford University, USA.

Appendix: Fokker–Planck Equation

A conservation law for $\mathcal{F}$ can be derived by considering mass balance of phase-a in an infinitesimal control volume of size $(d\boldsymbol{x}dc)$, which leads to the MDF-transport equation

$$\frac{\partial \mathcal{F}}{\partial t} + \frac{\partial}{\partial x_i}\left\{D_i^{\boldsymbol{x}}\mathcal{F}\right\} + \frac{\partial}{\partial c}\left\{D^c\mathcal{F}\right\} = \frac{\partial^2}{\partial x_i \partial x_j}\left\{D_{ij}^{\boldsymbol{x},\boldsymbol{x}}\mathcal{F}\right\} + \frac{\partial^2}{\partial c \partial c}\left\{D^{c,c}\mathcal{F}\right\} + \frac{\partial^2}{\partial x_i \partial c}\left\{D_i^{\boldsymbol{x},c}\mathcal{F}\right\} + Q\mathcal{F}. \tag{42}$$

This is a Fokker–Planck equation (Gardiner 2004) with the coefficients defined by

$$
\begin{aligned}
D_i^x &= \lim_{\Delta t\to 0}\frac{1}{\Delta t}\,\langle\{X_i(t+\Delta t)\;-\;X_i(t)\}|\,x,a,c\rangle\,,\\
D^c &= \lim_{\Delta t\to 0}\frac{1}{\Delta t}\,\langle\{C(t+\Delta t)\;-\;C(t)\}|\,\boldsymbol{x},a,c\rangle\,,\\
D_{ij}^{x,x} &= \lim_{\Delta t\to 0}\frac{1}{2\Delta t}\,\big\langle\{X_i(t+\Delta t)-X_i(t)\}\left\{X_j(t+\Delta t)-X_j(t)\right\}\big|\,x,a,c\big\rangle\,,\\
D^{c,c} &= \lim_{\Delta t\to 0}\frac{1}{2\Delta t}\,\big\langle\{C(t+\Delta t)-C(t)\}^2\big|\,x,a,c\big\rangle\,,\\
D_i^{x,c} &= \lim_{\Delta t\to 0}\frac{1}{2\Delta t}\,\langle\{X_i(t+\Delta t)-X_i(t)\}\{C(t+\Delta t)-C(t)\}|\,x,a,c\rangle
\end{aligned}
\tag{43}
\tag{44}
$$

and

$$
Q=\frac{1}{M(t)}\lim_{\Delta t\to 0}\frac{1}{\Delta t}\,\langle\{M(t+\Delta t)-M(t)\}|\,x,a,c\rangle\,. \tag{45}
$$

To evaluate these coefficients, we need the Lagrangian evolutions of the stochastic variables $\boldsymbol{X}(t)$, $C(t)$ and $M(t)$. For $\boldsymbol{X}(t)$ and $C(t)$, these are given by Eq. 2 and Eq. 17, respectively:

$$
\mathrm{d}X(t)=U(t)\mathrm{d}t+\sqrt{2\Gamma|U(t)|}\mathrm{d}W(t)\quad\text{and} \tag{46}
$$

$$
\mathrm{d}C(t)=-\left\{\frac{(1-C)(C-C^{\mathrm{eq}})}{\tau_{\mathrm{d}}}\mathrm{d}t+\frac{(1-C)(C-\overline{C|a=2})}{\tau_{\mathrm{m}}}\mathrm{d}t\right\}\delta_{A(t)2}. \tag{47}
$$

The evolution for M can be obtained by combining Eqs. 14 and 21:

$$
\begin{aligned}
\frac{1}{M(t)}\frac{\mathrm{d}M(t)}{\mathrm{d}t} &= -\delta_{A2}\frac{(C(t)-C^{\mathrm{eq}})}{\tau_{\mathrm{d}}}-\delta_{A2}\frac{(C(t)-\overline{C(t)|a=2})}{\tau_{\mathrm{m}}}\\
&\quad+\delta_{A1}\frac{\rho_2 S_2}{\rho_1 S_1}\frac{(\overline{C|a=2}-C^{\mathrm{eq}})}{\tau_{\mathrm{d}}}.
\end{aligned}
\tag{48}
$$

Using Eqs. 46, 47, and 48 we obtain

$$
D_i^x=-\frac{k_{\mathrm{r}_1}k}{S_1\phi\mu_1}\left(\frac{\partial p_1}{\partial x_i}+\rho_1 g e_{z_i}\right)\delta_{a1}-\frac{k_{\mathrm{r}_2}k}{S_2\phi\mu_2}\left(\frac{\partial p_2}{\partial x_i}+\rho g e_{z_i}\right)\delta_{a2}, \tag{49}
$$

$$
D^c=-\frac{(1-c)(c-C^{\mathrm{eq}})\delta_{a2}}{\tau_{\mathrm{d}}}-\frac{(1-c)(c-\overline{C|a=2})\delta_{a2}}{\tau_{\mathrm{m}}}, \tag{50}
$$

$$
D_{ij}^{x,x}=\langle\Gamma|U||\,x,a,c\rangle\,\delta_{ij},\;D^{c,c}=D_i^{x,c}=0 \tag{51}
$$

and

$$
Q=-\delta_{a2}\frac{(c-C^{\mathrm{eq}})}{\tau_{\mathrm{d}}}-\delta_{a2}\frac{(c-\overline{C|a=2})}{\tau_{\mathrm{m}}}+\delta_{a1}\frac{\rho_2 S_2}{\rho_1 S_1}\frac{(\overline{C|a=2}-C^{\mathrm{eq}})}{\tau_{\mathrm{d}}}. \tag{52}
$$

References

Ahlstrom, S., Foote, H., Arnett, R., Cole, C., Serne, R.: Multi-component mass transport model: Theory and numerical implementation. In: Rep. BNWL-2127 (1977)

Aziz, K., Settari, A.: Petroloeum Reservoir Simulation. Applied Science Publisher, London (2002)

Bachu, S.: Sequestration of CO_2 in geological media in response to climate change: capicity of deep saline aquifers to sequester CO_2 in solution. Energy Convers. Manag. **44**, 3151–3175 (2003)

Bear, J.: Dynamics of Fluids in Porous Media. Dover Publications, Inc., New York (1972)
Bear, J.: Hydraulics of Groundwater. Dover Publications, Inc., New York (1979)
Blunt, M., King, P.: Macroscopic parameters from simulations of pore scale flow. Phys. Rev. A **8**, 4780–4787 (1990)
Blunt, M., King, P.: Relative permeabilities from two- and three-dimensional pore-scale network modeling. Transp. Porous Med. **6**, 407–433 (1991)
Blunt, M., King, M., Scher, H.: Simulation and theory of 2-phase flow in porous media. Phys. Rev. A **46**, 2004–2011 (1992)
Blunt, M., Jackson, M.D., Piri, M., Valvatne, P.H.: Detailed physics, predictive capabilities and macroscopic consequences for pore-network models of multiphase flow. Adv. Water Resour. **25**, 1069–1089 (2002)
Chandler, R., Koplik, J., Lerman, K., Willemsen, J.F.: Capillary displacement and percolation in porous media. J. Fluid Mech. **119**, 249–267 (1982)
Dahle, H., Espendal, M., Ewing, R., varied, O.S.: Characteristic adaptive subdomain methods for reservoir flow problems. Numer. Methods Part. Diff. Equ. **6**, 279–309 (1990)
Dahle, H., Ewing, R., Russell, T.: Eulerian-Lagrangian localized adjoint method for a nonlinear advection-diffusion equation. Comput. Methods Appl. Mech. Eng. **34**, 1051–1069 (1995)
Gardiner, C.W.: Handbook of Stochastic Methods. Springer, New York (2004)
Heinz, S.: Statistical Mechanics of Turbulent Flows. Springer, New York (2003)
Hewett, T., Yamada, T.: Theory for the semi-analytic calculation of oil recovery and effective relative permeabilities using streamtubes. Adv. Water Resour. **20**, 279–292 (1997)
Jenny, P., Pope, S., Muradoglu, M., Caughey, D.: A hybrid algorithm for the joint pdf equation of turbulent reactive flows. J. Comput. Phys. **166**, 218–252 (2001)
Kinzelbach, W.: Numerische Methoden zur Modellierung des Transports von Schadstoffen im Grundwasser. Oldenbourg Verlag, München (1992)
Lenormand, R., Touboul, E., Zarcone, C.: Numerical-models and experiments on immiscible displacement in porous-media. J. Fluid Mech. **189**, 165–187 (1988)
Muskat, M.: Physical Princples of Oil Production. McGraw-Hill, London (1949)
Okabe, H., Blunt, M.J.: Prediction of permeability for porous media reconstructed using multiple-point statistics. Phys. Rev. E **70**, 066,135–066,145 (2004)
Pope, S.: Pdf methods for turbulent reactive flows. Prog. Energy Combust. Sci. **11**, 119–192 (1985)
Prickett, T., Naymik, T., Longquist, C.: A random walk solute transport model for selected groundwater quality evaluations. In: Rep. I-11 (1981)
Pruess, K., Garcia, J.: Multiphase flow dynamics during CO_2 disposal into saline aqifers. Environ. Geol. **42**, 282–295 (2002)
Rembold, B., Jenny, P.: A multiblock joint pdf finite-volume hybrid algorithm for the computation of turbulent flows in complex geometries. J. Comput. Phys. **220**, 59–87 (2006)
Riaz, A., Hesse, M., Tchelepi, H.A., Orr, F.M.: Onset of convection in a gravitationally unstable diffusive boundary layer in porous media. J. Fluid Mech. **548**, 87–111 (2006)
Tyagi, M., Jenny, P., Lunati, I., Tchelepi, H.A.: A stochastic, Lagrangian modeling framework for multi-phase flow in porous media. J. Comput. Phys. **227**, 6696–6714 (2008)
Whitaker, S.: Flow in porous media i: a theoretical derivation of Darcy's law. Transp. Porous Med. **1**, 3–25 (1986a)
Whitaker, S.: Flow in porous media ii: the governing equations for immiscible, two-phase flow. Transp. Porous Med. **1**, 105–125 (1986b)